Contents lists available at ScienceDirect

Materials Science & Engineering A

Strong grain size effect on tensile behavior of the body-centered-cubic Ti–30Zr–5Mo alloy with stress-induced α′ martensitic transformation

Chenyang Wu [a], Xiaoli Zhao [a,b,c,*], Mengrui Zhang [a], Hideki Hosoda [d], Takayoshi Nakano [e], Mitsuo Niinomi [e,f], Nan Jia [a], Zhiwen Shao [g], Deliang Zhang [a]

[a] School of Materials Science and Engineering, Northeastern University, Shenyang, 110819, PR China
[b] National Frontiers Science Center for Industrial Intelligence and Systems Optimization, Northeastern University, Shenyang, 110819, PR China
[c] Key Laboratory of Data Analytics and Optimization for Smart Industry (Ministry of Education), Northeastern University, Shenyang, 110819, PR China
[d] Institute of Innovative Research (IIR), Tokyo Institute of Technology, Yokohama, 226-8503, Japan
[e] Division of Materials and Manufacturing Science, Graduate School of Engineering, Osaka University, 2-1, Yamadaoka, Suita, Osaka, 565-0871, Japan
[f] Institute for Materials Research, Tohoku University, Sendai, Miyagi, 980-8577, Japan
[g] Inner Mongolia Metallic Material Research Institute, Baotou, Inner Mongolia, 83102, PR China

ARTICLE INFO

ABSTRACT

In this study the grain size effect on mechanical properties of a body-centered-cubic Ti–30Zr–5Mo alloy was investigated. Double yielding behavior in the stress-strain curves and four-stage behavior in the strain hardening rate curves can be seen in all Ti–30Zr–5Mo materials with different average grain sizes ranging from 6 to 475 μm, which is attributed to the occurrence of the stress-induced α′ transformation. The static Hall-Petch coefficient (k) for phase transformation was calculated to establish the relationship between grain size and trigger stress of the various materials. With the increase of strain, the hindrance of α′/β grain boundaries and α′/α′ grain boundaries to dislocations gradually replaced β/β grain boundaries, thus the work hardening ability and k value changed. β grains were segmented by α′ martensite, resulting in a dynamic Hall−Petch effect. Combined with a large stress field in the fine-grained materials with an average grain size of 6 μm, the highest work hardening rate with a value of 13 GPa was obtained. As the β grain size increased, the ultimate strength gradually decreased, while both trigger stress of the stress-induced α′ transformation and elongation fluctuated. The trigger stress can be adjusted between 211 and 464 MPa by controlling the grain size. The grain size has little effect on the amount of the stress-induced α′ phase. With a high trigger stress of 464 MPa in the material with the finest grains, the excellent ductility of 21% is obtained. The best comprehensive mechanical properties with a strength-ductility index value of 252 MPa is obtained in the material with an average grain size of 113 μm.

1. Introduction

The development of titanium (Ti) and its alloys plays a very important role in reaching the goal of carbon neutrality and carbon peaking. The application of those materials in aerospace and biomedical fields also has a promising future due to their high strength, good corrosion resistance and biocompatibility [1] [–] [3]. Currently, metastable β Ti alloys become popular because of their good workability and the overall excellent mechanical properties that can be obtained through forging and heat treatments [4]. The deformation mechanisms of metastable β Ti alloys mainly include martensitic transformation from β (body-centered cubic) to α′ (hexagonal close packed) and from β to α″ (orthorhombic)

[5], mechanical twinning [6] and dislocation slip [7]. The refinement of grain size, which may simultaneously improving strength and ductility, plays a crucial role in improving the properties of titanium alloys. Further, the grain size of β phase is an important variable that affects the deformation mechanism and behavior. Therefore, adjusting the grain size of β phase is crucial to optimize the properties of metastable β titanium alloy. However, since the body-centered-cubic structure with low packing density shows a higher diffusion rate at high temperature, it is difficult to refine the grain size. The common methods to prepare fine-grained metallic materials include severe plastic deformation and cold rolling plus annealing [8] [–] [11]. However, the severe plastic deformation is difficult for large scale fabrication. In steels and some

---

titanium alloys, the stress-induced martensite transformation and its reverse transformation (SIMRT) is an efficient method for refining grain size to improve properties [12]. Schino et al. proposed that the combination of cold rolling and annealing process to prepare ultrafine grained austenitic stainless steel should satisfy the following two conditions: (1) During the cold rolling process, all metastable austenite needs to be transformed into martensite; (2) Reverse phase transformation annealing must be carried out under low temperature conditions to prevent grain growth [13]. Ma et al. successfully prepared austenitic steel with a grain size of 100 nm through repeated cold rolling and annealing, and found that its mechanical properties were greatly improved [14]. Compared with severe plastic deformation, it is simpler and more convenient to use SIMRT to refine the grain size by cold rolling and annealing. It provides a way to refine the metastable BCC titanium alloy with martensitic transformation. Metastable β Ti–30Zr–5Mo alloy has similar characteristics to metastable austenitic steel, in which the abundant transformation from β to α′ martensite occurs during deformation. Therefore, it is promising to refine Ti–30Zr–5Mo alloy through cold rolling and annealing by SIMRT.

The stress-induced martensite transformation in metastable β Ti alloys generally manifests a typical double yielding or strain plateau region in the engineering stress-strain curves [12,15]. The dominant factor that affects the double yielding or strain plateau region is the trigger stress (TS) for the stress-induced martensite transformation [16]. According to the Conside're criterion, the high uniform elongation requires the high work hardening during tensile deformation. In order to obtain excellent combination of strength and ductility in metastable β titanium materials with different grain size, it is significant to explore the influencing factors on the trigger stress and work hardening rate.

Hall-Petch coefficient (k) is an important parameter in Hall-Petch relationship which describes the boundaries hardening effect. However, most of Hall-Petch coefficient is deduced in the alloys with dislocation slip. In metastable titanium alloys, the deformation mechanisms vary with changing the β stabilizing elements. Besides the initial grain size difference, the dynamic refinement occurs during the following phase transformation or twinning. Kai Yao et al. established a static and dynamic Hall-Petch relationship for the change in Hall-Petch coefficient caused by twinning [17]. However, the twin boundaries can be assumed as grain boundaries as the matrix and twin have the same crystal structure with different misorientations. And the results show that the Hall-Petch coefficient (k) for twinning is larger than that for dislocation slip. It is crucial to find the Hall-Petch coefficient (k) for martensitic transformation and interpret if it varies during the deformation as the phase boundaries are different from twin boundaries and grain boundaries due to the crystal structure difference.

In this study, Ti–30Zr–5Mo materials with different grain sizes in a large range were prepared through SIMRT and simple heat treatments. The change of trigger stress and work hardening ability of Ti–30Zr–5Mo materials with different grain sizes were analyzed by calculating the Hall-Petch coefficient (k) combined with the Crussard-Jaoul (C-J) analysis. The effect of grain size on deformation behavior in the Ti–30Zr–5Mo materials with different grain sizes at room temperature was revealed.

2. Materials and methods

2.1. Materials

Ti–30Zr–5Mo alloy was triply melted by consumable vacuum arc-melting sponge Ti, sponge Zr, and Ti–32Mo master alloy. The ingot was homogenized at 1100 °C for 6 h in vacuum and then forged at 1100 °C and air cooled to room temperature. Differential scanning calorimetry (DSC, Netzsch STA449F3) measurements were carried out at 20 °C/min. According to the DSC results, as shown in Fig. 1, the α to β phase transformation temperature of Ti–30Zr–5Mo alloy was determined to be approximately 700 °C. To obtain body-centered-cubic

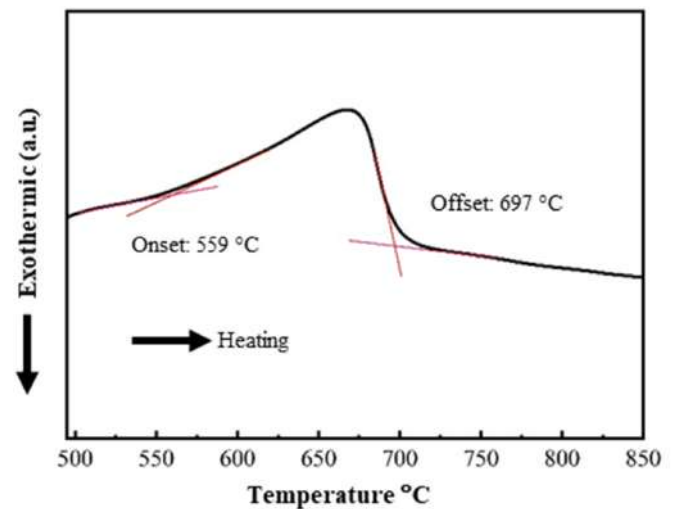**Fig. 1.** DSC curve of the Ti–30Zr–5Mo alloy.

Ti–30Zr–5Mo materials with different β grain sizes, different heat treatment processes were conducted, as shown in Fig. 2a. The samples were solution treated at varied temperatures (700–950 °C) in β phase region with different annealing times (30–60 min) in vacumm and followed by water quenching. SIMRT was used to obtain finer grain sizes. The ingots were cold rolled with a reduction ratio of 30%, and then solution treated at 700 °C for 2 min. The above process is one loop, and all the processes are shown in Fig. 2b.

2.2. Experimental methods

Tensile specimens with a total length of 40 mm, gauge a length of 13 mm, a width of 3 mm, and a thickness of 1.5 mm were prepared by electrical discharge wire cutting. The SHIMADZU AG-XPLUS 100 KN tensile testing machine was used for tensile tests at room temperature with a strain rate of 3×10^{-4} s^{-1}. Three samples of each grain size were prepared to minimize errors. Before optical microscopy observation using an optical microscope (OM, ZESS AXIO), the materials were mechanically polished and then chemically etched using a solution of 3.5 pct hydrofluoric acid (HF), 10 pct nitric acid (HNO3) and 86.5 pct distilled water (H2O). The phase constitutions of the tensile materials before and after deformation were determined by X-ray diffractometer (XRD, Smart Lab). The samples after deformation for XRD acquisition are taken near the fracture of the tensile specimens after fracture. In order to compare the amount of the martensitic transformation quantitatively, the sample size kept uniform. In-situ tensile tests in scanning electron microscopy (SEM, JEOL JSM-7001F) and electron back-scattered diffraction (EBSD, Oxford instrument Symmetry) systems were used to analyze the microstructural evolution of materials during tensile deformation.

3. Results

3.1. Microstructure

Fig. 3 is the optical micrographs of the Ti–30Zr–5Mo materials subjected to different processing routes. All materials are comprised of equiaxed grains with different grain sizes. Since the heating temperatures are above the β transus temperature, the α phase is completely transformed into the β phase. The grain size (grain diameter) is refined from 475 to 136 μm (Fig. 3a and b) as the temperature decreases from 950 to 750 °C for 60 min. After heat treatment at 950 °C for 60 min, the average grain size of β phase is 475 μm. After heat treatment at 850, 800 and 750 °C, the refinement rates are 36.8%, 53.7% and 71.4%, and the
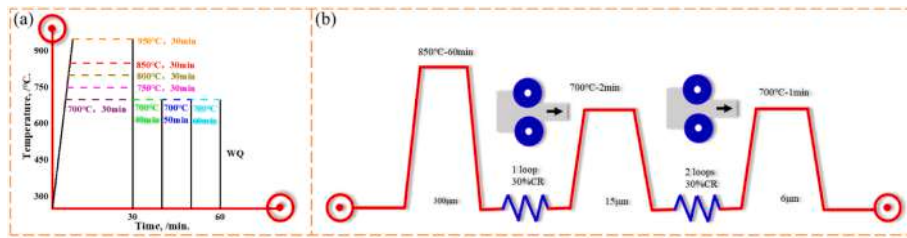
Fig. 2. Schematic illustration of (a) solution treatment process and (b) SIMRT process applied to the Ti–30Zr–5Mo alloy for grain size refinement.
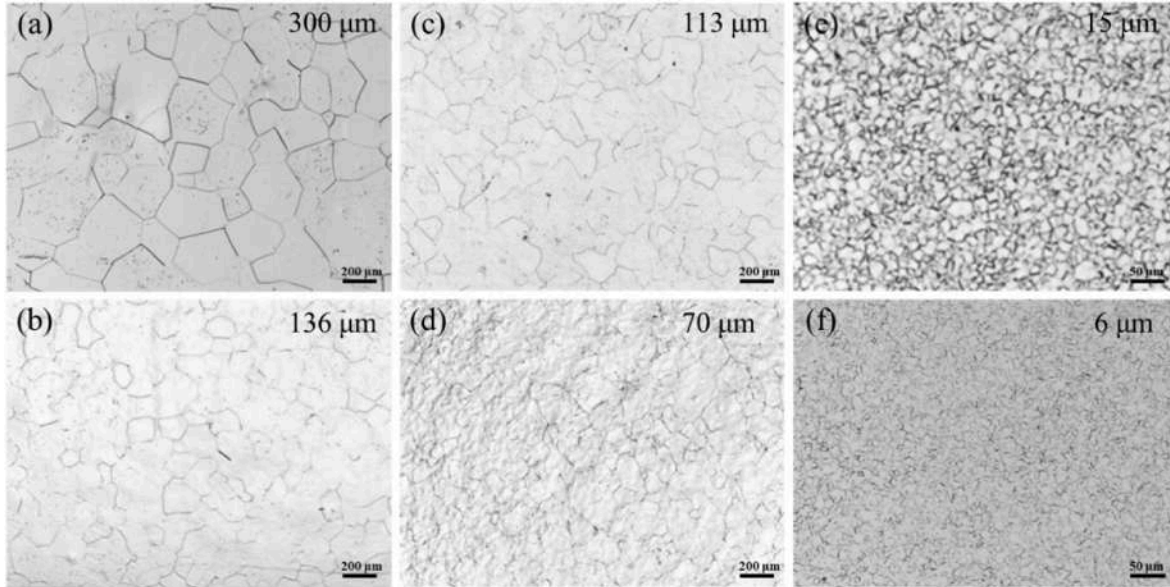

Fig. 3. OM micrographs of the materials after annealing at (a) 950 °C, (b) 750 °C for 60 min, at 700 °C for (c) 60 min and (d) 30 min, and after SIMRT processing for (e) 1 loop, (f) 2 loops.

average grain sizes are 300, 220 and 136 μm, respectively. This provides a large span of grain size control. To refine the grain size further, average grain sizes of 70 and 113 μm (Fig. 3c and d) are obtained by heating at 700 °C for 30 and 60 min, respectively. After heat treatment at 700 °C for 60min., the average grain size of β phase is 113 μm, and with the time decreasing to 50, 40 and 30 min, the grain size of β is refined to 108, 85 and 70 μm, respectively, compared with the material with grain size of 113 μm, the refinement rates are 4.4%, 24.8% and 38.1%, respectively. This shows that the grain size of Ti–30Zr–5Mo metastable β titanium alloy can be manipulated by simply controlling the heat treatment parameters. Combined with SIMRT, the average grain size decreases from 300 to 6 μm (Fig. 3e-f) with increasing number of loops from 0 to 2. X.J. Jiang et al. [12] also reported that grain size refinement was achieved using a multiloops of deformation with low strain and annealing. It is confirmed that SIMRT is an effective way for grain refinement in metastable β alloys.

Fig. 4 shows the variation curves of the β grain size with temperature and annealing time for Ti–30Zr–5Mo alloy. It is obvious that temperature is more effective for the grain coarsening. As the temperature increases, the grain size increases and tends to grow exponentially. The β grain size increases with increasing annealing time; when the annealing time is within 30–50 min, the grain size grows faster; however, when the annealing time exceeds 50 min, the grain growth rate slows down.

The crystallographic orientation has significant effect on the deformation mechanism and mechanical properties. The pole figure of the EBSD is presented to analyze the texture density of Ti–30Zr–5Mo alloy with different grain sizes, as shown in Fig. 5. In Fig. 5 (a), the orientation is randomly distributed in 6 μm material, the maximum polar densities in {100}, {110} and {111} poles are 5.58, 3.88, 4.14, respectively,
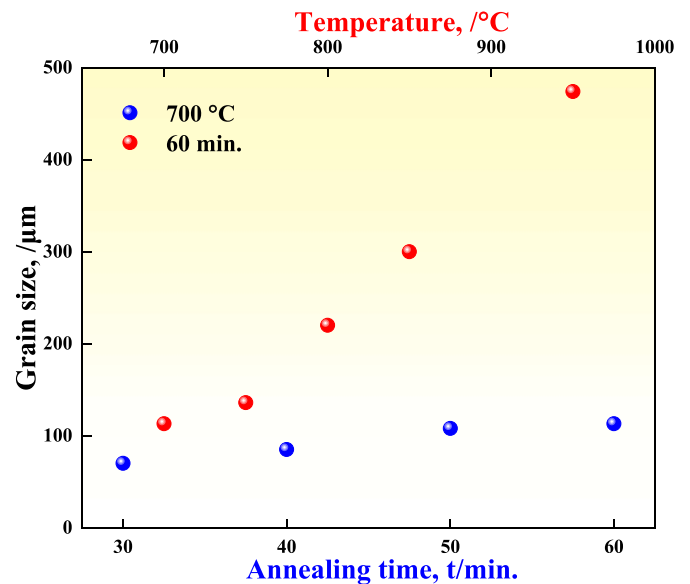

Fig. 4. Dependence of grain size on annealing temperature and annealing time.

indicating the texture in this region is weak. The scattered poles can be observed in 15 μm material shown in Fig. 5 (b), and the maximum polar densities are in {100}, {110} and {111} poles are 8.85, 5.78, 7.62, respectively, demonstrating some weak texture in this region. For the
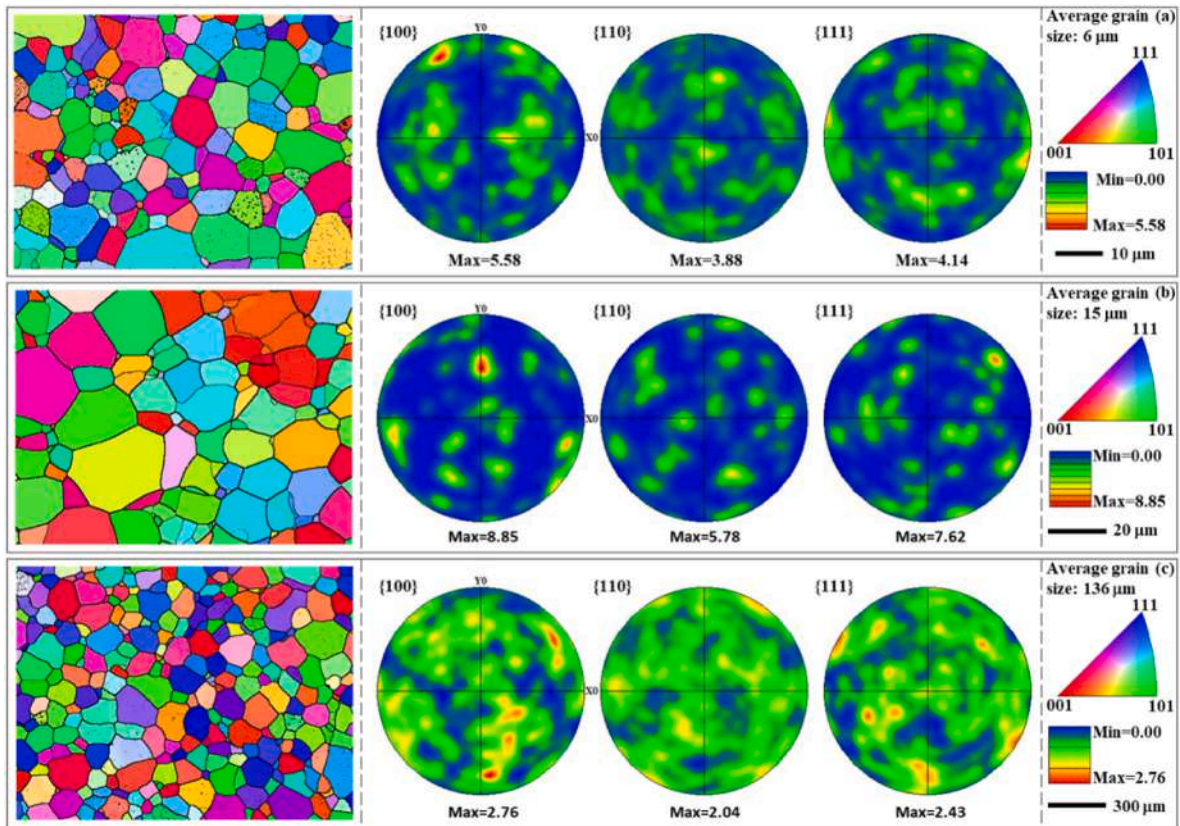
Fig. 5. EBSD analysis revealing the texture strength of the Ti–30Zr–5Mo alloy materials with different grain size (a) 6 μm (b) 15 μm (c) 136 μm.

115 μm material shown in Fig. 5 (c), the pole distributions are fairly random, and the maximum polar density are merely 2.76, 2.04, and 2.43, respectively, imply the weak texture in this region. Therefore, the effect of crystallographic orientation difference between the materials with different grain size can be ignorable in this study.

3.2. Mechanical properties

Fig. 6 (a) shows the engineering tensile stress (s)–strain (e) curves of Ti–30Zr–5Mo materials with different β grain sizes. All the curves show a typical double yielding phenomenon, which is commonly associated with stress-induced martensitic transformation. Further, an abnormally high trigger stress is observed when the grain size is smaller than 15 μm. The curves can be divided into four stages according to the slope change [18,19]. The trigger stress of the transformation from β phase to α′ phase can be defined as the intersection of the stress value corresponding to the

stage I tangent and stage II tangent. It fluctuates between 211 ± 6 and

Table 1
Tensile mechanical properties of Ti–30Zr–5Mo materials with various grain sizes.

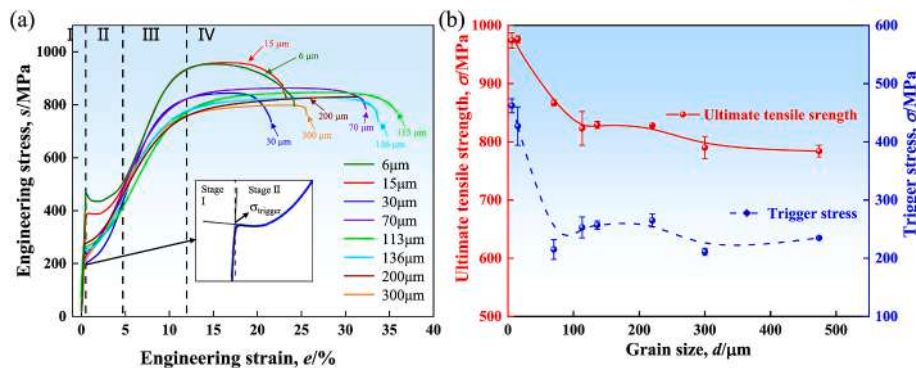| Grain size (μm)	Yield strength (YS, MPa)	Trigger stress (TS, MPa)	Ultimate tensile strength (UTS, MPa)	TS/ UTS	Elongation (%)
6	866 ± 3	464 ± 12	976 ± 6	0.47	22 ± 3.2
15	849 ± 30	427 ± 33	974 ± 13	0.44	21 ± 0.6
70	680 ± 2	215 ± 17	867 ± 5	0.25	27 ± 2.8
113	639 ± 23	253 ± 18	823 ± 29	0.31	33 ± 1.7
136	646 ± 8	257 ± 7	829 ± 6	0.31	31 ± 5.1
220	628 ± 6	265 ± 11	828 ± 1	0.32	34 ± 0.7
300	617 ± 15	211 ± 6	790 ± 19	0.27	23 ± 4.7
474	574 ± 14	235 ± 2	784 ± 10	0.30	31 ± 1.4

Fig. 6. (a) Engineering stress–strain curves of the Ti–30Zr–5Mo materials with various grain sizes and (b) grain size effects on the ultimate tensile strength and trigger stress of the alloys.

464 ± 12 MPa in the materials with grain size ranging from 6 to 474 μm as shown in Table 1. The variation in the trigger stress under different grain sizes is illustrated in Fig. 6 (b). In the region at stage III, which represents elastic deformation of the α' phase and β phase, a 0.2% proof stress (yield strength: YS) is obtained and shown in Fig. 7. The yield strength and ultimate tensile strength (UTS) increase from 574 ± 14 to 866 ± 3 MPa, respectively and from 784 ± 10 to 976 ± 6 MPa, respectively with decreasing grain size.

In addition, the ductility of the Ti–30Zr–5Mo alloy fluctuates with decreasing grain size. Fig. 7a shows that the elongation to fracture of the Ti–30Zr–5Mo alloy remains 30%–34% when the grain size is refined from 474 to 113 μm, except for the 300 μm material. However, with the grain size refining to 6 μm, the elongation of the alloy decreases from 34% to 21%. The phase transformation and twinning can close cracks, relieve stress concentration during deformation, and lead to an enhancement of ductility [20]. Therefore, Ti–30Zr–5Mo alloy has excellent elongation to fracture no less than 21%. On the other hand, as the grain size decreases from 113 to 6 μm, the β grains are segmented by the α' martensite laths into smaller domains with increasing the strain, which reduce the ability to accommodate dislocations. Although higher work hardening ability is obtained in 6 μm material, the refinement hardening increases the flow stress, which makes intersection of work hardening curve and true stress-strain curve at smaller strains, thereby weaken the plastic instability. Thus, the elongation of the Ti–30Zr–5Mo alloy shows a decreasing trend as the grain size decreases to 6 μm.

The strength-ductility index (SDI) is defined as (UTS-YS) × Plastic strain, which is generally used to evaluate the increase in toughness of materials [21]. For a better comparison, the SDI values are illustrated in Fig. 7. As seen in Fig. 7 (a), the large SDI values (over than 220 MPa) can be obtained for medium grained materials (the grain sizes in the range of 113–220 μm). The Ti–30Zr–5Mo material with grain size of 113 μm achieves the largest SDI value of 252 MPa. Compared with other metastable β titanium alloys [1,22–24], it is only lower than that of the Ti–15Mo-0.1O alloy with twinning during deformation.

3.3. Work hardening behavior

Fig. 8 (a) shows the work hardening rate (dσ/dε) curves of the Ti–30Zr–5Mo materials with different grain sizes. They can be divided into four stages: (I) Elastic deformation region, where the strain hardening rate curves decrease rapidly; (II) Strain hardening rate increasing region; (III) Strain hardening rate decreasing region, which forms a "Hump" with the second region; and (IV) Necking and fracture region. The strength, ductility, toughness and deformability of materials are intimately related to strain hardening characteristics, and the content of martensite also leads to a higher work hardening ability [25]. In Fig. 8 (a), the stage I corresponds to the dynamic softening effect due to the α' martensite transformation, which means low work hardening rate. With the decrease of grain size, the minimum work hardening rate of the

Ti–30Zr–5Mo alloy materials decreases from 1.86 GPa (474 μm) to −0.71 GPa (6 μm). In the stage II, the work hardening is dominated by the strengthening effect of α' martensite phase, at which time the work hardening rate increases. The maximum work hardening rate of the Ti–30Zr–5Mo materials increases from 7.83 GPa (474 μm) to 13.6 GPa (6 μm) with the decrease of grain size. In the stage III, the behavior of materials begins to resemble that of single-phase materials again, which means the work hardening rate begins to decrease. In other materials with similar work hardening rate curves, there is also a work hardening behavior in which the rapid decrease reaches the minimum value, then reaching the maximum value and finally to necking. Therefore, the work hardening behavior of the Ti–30Zr–5Mo materials is enhanced with the decreasing of grain size.

Usually, in order to discuss the work hardening behavior of metals, the empirical equations and the analyses based on these equations are used. Among these most popular are Hollomon analysis, and Crussard–Jaoul (C–J) analysis based on Ludwik and Swift equations, popularly known as differential C-J ($D_{C–J}$) and modified C-J ($M_{C–J}$) techniques, respectively [26]. In titanium alloys, $D_{C–J}$ analysis (i.e., ln (dσ/dε) vs. ln ε) is useful for showing the relative changes in the work hardening behavior over a range of strains, especially in materials that exhibit microstructural evolutions (i.e., mechanical twinning and martensite transformation) during deformation [27,28]. In this analysis, a change in the slope of a line segment in C–J curve is dependent on the strengthening mechanism and the material type. Concerning strengthening mechanism, a very low slope of a line segment in C–J plot indicates a relatively rapid decrease in the work hardening rate with increasing strain or a high rate of dynamic recovery. Conversely, when the slope of a line segment in the C–J plot shows a larger value, it indicates that there is a relatively slow decrease in the work hardening rate (e.g., as a result of the strengthening effect due to formation of martensitic transformation or twinning).

In Fig. 8 (b), the work hardening characteristics of the materials with grain sizes of 15, 113, 200 and 300 μm is shown in C–J type plots, which is obtained from the following equation:

$$\ln\left(\frac{d\sigma}{d\varepsilon}\right) = \ln(kn) + (n-1)\ln\varepsilon \qquad (1)$$

where n and k are the work hardening exponent and material constant, respectively. n is useful for showing the variations in the work hardening behavior. The values of plastic strain (ε_I, ε_{II}, and ε_{III}) of each stage, the slopes (n_I, n_{II} and n_{III}) of each stage and the transition strains ($\varepsilon_{I–II}$, and $\varepsilon_{II–III}$) between the stages of each curve base on the C–J analysis are listed in Table 2.

Fig. 8 (b) and the detailed information in Table 2 show that at the first stage with n_I ranging from −1.83 to −7.24, the n_I value decreases with decreasing the grain size. The coarse-grained materials have the highest value of −1.83. This indicates that the work hardening of fine-grained material at stage I is lower (i.e., a relative rapid decrease in
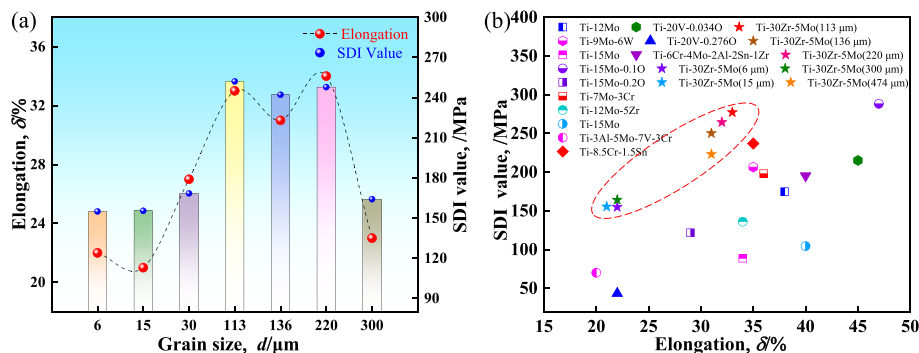

Fig. 7. (a) SDI values of the Ti–30Zr–5Mo materials with various grain sizes and (b) comparison of the SDI values of studied materials and other metastable β titanium alloys [1,22–24].
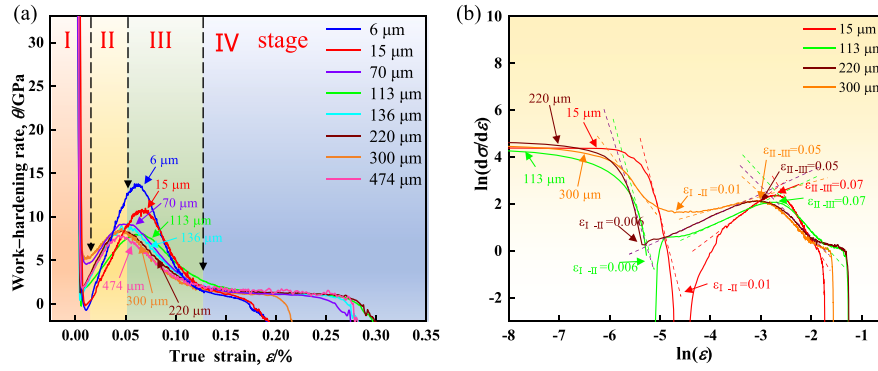
Fig. 8. (a) The strain hardening rate curves of the Ti–30Zr–5Mo materials with different grain sizes and (b) ln(dσ/dε) vs. lnε for the materials obtained from C-J analysis.

Table 2
The values of true strain (ε_I, ε_{II} and ε_{III}), work hardening exponent (n_I, n_{II} and n_{III}) at each stage and the transition strains ($\varepsilon_{I\text{-}II}$ and $\varepsilon_{II\text{-}III}$) between the deformation stages of Ti–30Zr–5Mo materials with different grain sizes obtained from the C-J analysis.

Grain size (μm)	Stage I		$\varepsilon_{I\text{-}II}$	Stage II		$\varepsilon_{II\text{-}III}$	Stage III	
	ε_I	n_I		ε_{II}	n_{II}		ε_{III}	n_{III}
15	0.006	−7.24	0.01	0.030	2.63	0.07	0.119	−2.50
113	0.005	−6.94	0.006	0.023	2.01	0.07	0.122	−1.38
200	0.0038	−5.96	0.006	0.024	1.98	0.05	0.091	−1.14
300	0.0045	−1.83	0.01	0.021	1.60	0.05	0.084	−0.94

the work hardening rate) compared to the coarse-grained materials. They are complying with the work hardening rates shown in Fig. 8 (a). This is considered to related to the dynamic softening of stress-induced martensite transformation [29]. In all the materials with different grain sizes, the *n* values in stage II are larger than stage I and become positive, which indicates the increase of work hardening rate. This means that the hardening effect caused by the stress-induced phase transformation in the materials are larger than the softening effect. The fine-grained material has the largest value, indicating the work hardening of fine-grained material at stage II is higher (i.e., a relative increase in the work hardening rate) than those of coarse-grained materials. This is also consistent with the work hardening rate shown in Fig. 8 (a). The 6 μm material exhibits the largest work hardening value of 13.6 GPa. In stage III, the *n* value become negative again, and the *n* value increases with increasing the grain size, similar to that in Stage I. However, the *n* value is larger than in stage I, indicating the decreasing the work hardening rate in stage III is slower than in stage I, The deformation behavior is analogous to the deformation in single phase [27,30], the slow decrease stems from the stress-induced α′ phase.

Additionally, the onset of stress-induced α′ phase transformation in the coarse- and fine-grained materials is detected at plastic strain of 0.01

($\varepsilon_{I\text{-}II}$). It means that the initiation of Stage II in all the materials are similar, which evidencing that the deformation-induced phase transformation in the present alloy occurs before macro yielding by slip. The grain size has little effect on the critical plastic strain for deformation-induced phase transformation.

3.4. Deformed microstructure

The volume fractions of the α′ phase and the β phase of the Ti–30Zr–5Mo materials with different grain sizes after tensile deformation are calculated from the XRD results. It is obvious in Fig. 9 (a) that the materials with different grain sizes have distinct α′ martensite peaks, indicating a transformation from cubic β phase to hexagonal α′ phase during tensile deformation. The peaks of α′{101} and β{110} are sensitive to the volume fractions of the α′ phase and β phase, and the peak intensity of α′{101} is significantly higher than that of β{110}. The volume fraction of the α′ phase calculated by MDI Jade 6 is presented in Fig. 9 (b). The content of the α′ phase fluctuates between 70% and 80% with decreasing grain size. Therefore, grain size has little effect on the content of the transformed α′ phase at room temperature. Furthermore, because the phase transformation from β phase to α′ phase is basically
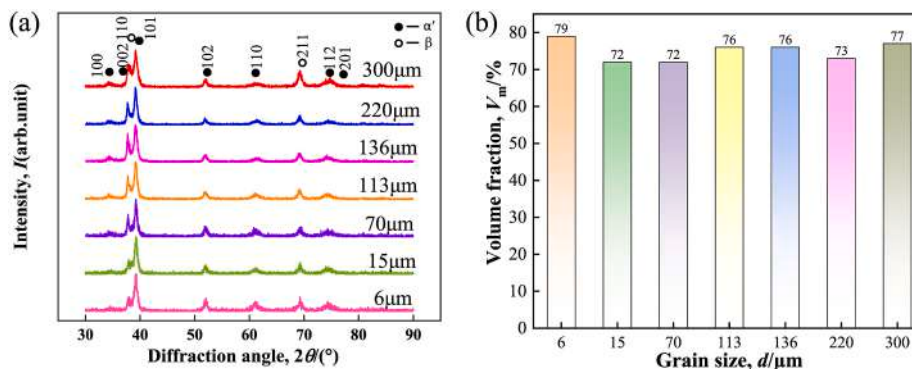

Fig. 9. (a) XRD spectra and (b) volume fraction of α′ martensite phase in the Ti–30Zr–5Mo materials with different grain sizes after tensile deformation.

completing at the end of stage III and the volume fraction fluctuates between 70% and 80%, the strain hardening rate is basically constant at the plateau region of stage IV, it is inferred that the martensite transformation is effective for improving the working hardening ability to retard the plastic instability.

4. Discussion

4.1. Refinement of the grain size

Although it is difficult to refine the grain size of materials with BCC structure due to the higher diffusion rate at high temperature, in this work, the grain size of body-centered-cubic Ti–30Zr–5Mo materials are adjusted from 6 to 475 μm by simple heat treatments. Gil et al. [31] reported that the grain growth rate of alloys followed an exponential trend with increasing temperature. Generally, temperature is the most important factor affecting grain growth kinetics and grain boundary activity, for which the following expressions are available [32]:

$$B = D_g / RT \qquad (2)$$

where B is the grain boundary activity, D_g is the grain boundary diffusion coefficient, R is the gas constant, and T is the temperature. The grain boundary diffusion coefficient can be further expressed as:

$$D_g = D_0 \exp\left(-Q_g / RT\right) \qquad (3)$$

Taking logarithms on both sides of the equation simultaneously, the following equation can be obtained.

$$ln\, D_g = ln\, D_0 - \frac{Q_g}{RT} \qquad (4)$$

where Q_g is the diffusion activation energy and D_0 is the diffusion constant and R is the gas constant, 8.314 J/(mol·K). As shown in Fig. 10, the relationship between grain size and temperature of Ti–30Zr–5Mo alloy can be obtained by fitting the linear relationship between $ln\, D_g$ and T^{-1} from Eq. (4) :

$$ln\, D_g = 12.49 - \frac{7686}{T} \qquad (5)$$

According to Eq. (5), the diffusion activation energy Q_g of Ti–30Zr–5Mo alloy is 63.9 (kJ/mol) in the selected heat treatment temperature range. Since grain growth is a thermal activation process, this activation energy is inversely proportional to the rate of grain
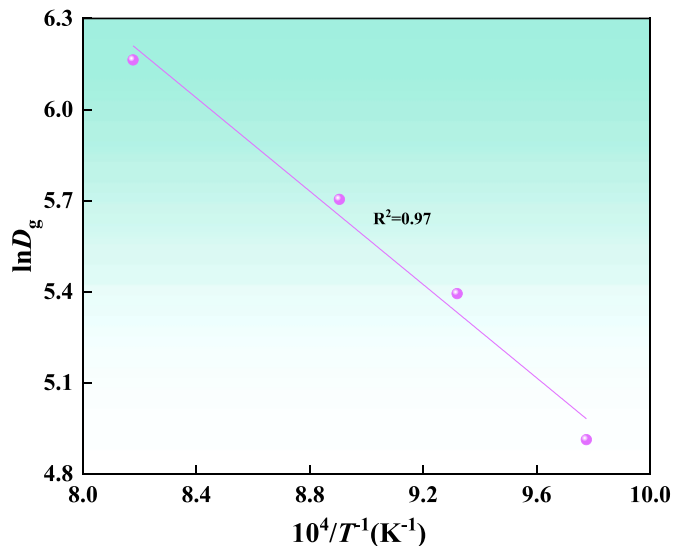
boundary movement. Ti–30Zr–5Mo alloy has lower activation energy compared with TG6 (Ti-5.8Al-4.0Sn-4.0Zr-0.7Nb-1.5Ta-0.4Si-0.06C) alloy (120.4–212.5 kJ/mol), Ti17 (Ti–5Al–2Sn–2Zr–4Mo–4Cr) alloy (290.5–378.5 kJ/mol), Ti–6Al–4V alloy (166.2 kJ/mol) and TC19 (Ti–6Al–2Sn–4Zr–6Mo) alloy (226.9 kJ/mol) [32,33]. Therefore, the grain growth rate of Ti–30Zr–5Mo alloy is faster. As the temperature increases, the rate of atomic diffusion is accelerated, the rate of grain boundary movement increases sharply with increasing temperature, and the grain growth rate is also accelerated.

However, varying the annealing time to achieve small-span grain size can be explained by traditional polycrystalline grain growth theory. The relationship between grain growth driving force (the chemical potential drop across a grain boundary) $\Delta\mu$ and grain size d can be quantitatively described by Gibbs-Thompson empirical equation [34]:

$$\Delta\mu = 4\Omega\gamma/d \qquad (6)$$

where Ω is the atomic volume and γ is the interfacial energy. It is inferred that the smaller the grain size, the higher the driving force of grain growth. When the annealing time is short, the large number of fine grains store abundant interfacial energy, providing driving force for grain growth, the grain size grows faster. However, with increasing the annealing time, the average grain size increases, and the grain growth rate $d\mathrm{D}/dt$ is positive but decreases steadily with time at a constant temperature.

In addition, metastable β Ti–30Zr–5Mo alloy has similar properties to metastable austenitic steel. The grains can be refined by cold rolling and annealing. The refinement process of metastable austenitic steel is divided into two steps: (1) transformation of metastable γ phase into α′ martensite phase by cold rolling, and (2) annealing at proper temperature, the reverse transformation of α′ martensite into γ phase occurs [14, 35]. During the cold rolling process, different sub-grains and dislocation cells were formed to adapt to the breakage of geometrically deformed grains, and the stress-induced α′ martensite transformation also occurred, the cold rolling reduction affects the internal defects and the entropy of deformation system, and then affects the reverse phase transformation and γ phase recrystallization. For titanium alloy, during the annealing, the proper temperature should be chosen for ensuring the α′→β reverse phase transformation and avoiding the rapid growth of β grains due to high diffusion rate at high temperature. In addition, if the annealing time is too short, the reverse phase transformation process may be insufficient, but too long time will lead to grain growth. Therefore, the optimization of cold rolling reduction, annealing temperature and time is crucial for the grain size refinement and need to be comprehensively considered through experiments. Even with the small activation energy, the grain size can be refined to 6 μm in Ti–30Zr–5Mo alloy with the SIMRT effect, confirming that SIMRT is an effective way to refine the metastable β titanium alloy.

4.2. The yield phenomena in the fine-grained alloys

It is noticed that the shape of the stress-strain curves in 6 μm and 15 μm materials differs from other materials with larger grain sizes. They show yielding phenomena, especially for 6 μm material. Because the shape of the stress-strain curve changes when the grain size is refined to 15 μm, we observe the in-situ microstructural evolution during deformation in 15 μm material, as shown in Figs. 11 and 12 using EBSD and SEM, respectively. It shows that the stress-induced α′ phase transformation occurs with a strain of 1%, corresponding to the onset of plastic deformation. Even before reaching the yield point, the stress-induced α′ phase can be observed in specific grains, as shown in Fig. 12. Therefore, we inferred that the stress drop in 6 μm material and stress plateau in 15 μm material are both related to the stress-induced α′ phase transformation.

Although Cottrell atmosphere-like adherence of small solutes to dislocations is one of the explanations for yielding phenomena, small
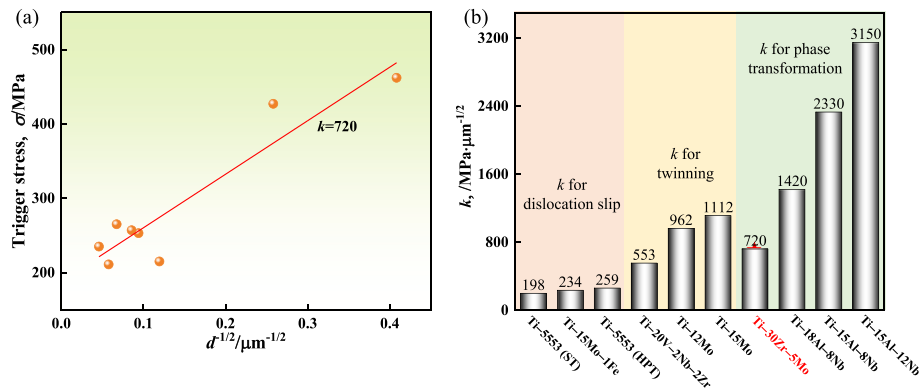

Fig. 10. Thermodynamics relationship between grain size ($\ln D_g$) and heat treatment temperature ($10^4/T$) of the Ti–30Zr–5Mo alloy.

Fig. 11. In-situ EBSD phase maps of the 15 μm material at (a) 0% and (b) 1% applied strains. (c) and (d) are the KAM maps corresponding to (a) and (b), respectively.
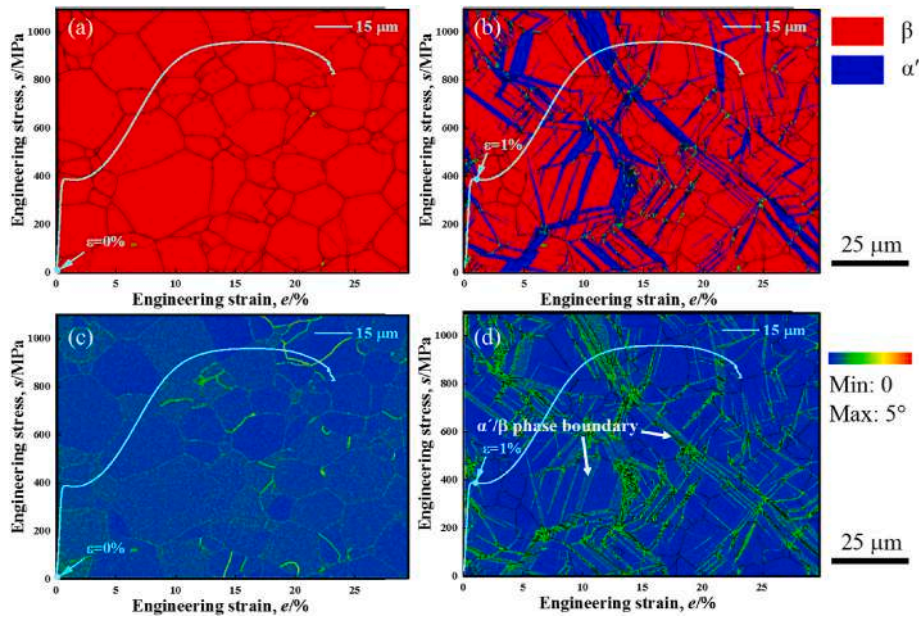

Fig. 12. Engineering stress-strain curves of the 15 μm grain-sized material and In-situ SEM images at different applied deformation stages: (a) 0.0028 strain, (b) 0.015 strain, (c) 0.059 strain and (d) after fracture.

solutes in this study are not assumed as the main reason for stress drop in 6 μm material or stress plateau in 15 μm material. As comparing with the coarse-grained materials, one or two loops of cold-rolling and solution treatment are conducted to refine the grain to 15 μm and 6 μm; the cold-rolling with a reduction ratio of 30% is done in the air, and time for solution treatment is within 2 min. Although the oxygen can diffuse to the matrix during the cold rolling and solution treatment, the slight reduction ratio and short annealing time prohibit the deeper diffusion of oxygen. Further, the surfaces with a thickness of more than 100 μm are removed after solution treatment, which prevents the possible effect of oxygen-rich surfaces on the tensile deformation behavior; the oxygen content of 6 μm material analyzed by the chemical method (He carrier fusion–infrared absorption method) is 0.12% (mass%), same to the coarse-grained material. Therefore, the effect of interstitial elements such as oxygen is not the main reason for the yield drop in this study. Such yielding phenomena are also reported in ultra-fine Cu and IF steel with low interstitial elements [36,37].

Similar to the dislocation slip mechanism [38], micro-yielding occurs before macro-yielding; the deformation is non-uniform at the beginning and starts locally in a portion of the gauge section. The stress at which a cluster of grains penetrates the surrounding elastic matrix determines the value of upper yield stress. The cluster size depends on the grain size,

grain size distribution, and orientation distribution of grains in poly-crystals. The phase transformation initiates in neighboring grains due to pile up stress concentration from the largest grains in the cluster. Initiating phase transformation across grain boundaries is difficult in smaller grains in a cluster. The size and distribution of smaller grains control the size of the cluster and the stress at which deformation spreads. The cluster size influences the local plastic strain rate at which deformation spreads. As the average grain size increases, per unit change in the size of neighboring grains causes less change in the stress. For a given distribution of grain size, a small decrease in the size of neighboring grains does not require a greater increase in applied stress for the transfer of martensite transformation in the micro-yield region. In this process, a slight increase in stress can draw more neighboring grains into the clusters. Therefore, the size of the initial cluster before spreading is larger for coarse-grained material. As the cluster grows in the micro yield region, the stress concentration increases as a function of cluster size. Considering the random orientation of grains and the number of dislocation sources per unit volume to be uniform, the micro-yield region strain varies as d^3 with grain size and parabolically with applied stress. Thus, the stress at which the deformation spreads continuously, i. e., the upper yield stress, is used to be lower for coarse-grained material. The grain boundaries provide greater capability for dislocation

absorption or obstacles; due to the small grain boundaries area in coarse-grained material, the velocity of dislocations released at upper yield is less for coarse-grained material. Johnston-Gillman model ($v = (\tau/\tau_0)^n$) indicates that the velocity decrease corresponds to the decrease in stress. Therefore, materials with larger grains have lower upper yield stress and lesser yield drop. With decreasing the grain size, the stress plateau first appears in 15 μm material, and an obvious stress drop can be found in 6 μm material.

4.3. Static Hall-Petch relation by grain size dependency for martensite transformation

All studied Ti–30Zr–5Mo materials with different grain sizes exhibit SIMT. They have similar stress-strain curves, and their trigger stresses fluctuate between 211 and 462 MPa. The relationship between the trigger stresses of materials and grain size and Hall-Petch dependence on grain size in titanium alloys with dislocation slip has been explored in many researches [17,39]. The grain boundaries are effective barriers for dislocation slip and the dislocations pile up at the grain boundaries, which leads to stress concentration at boundaries. If the concentrated stress exceeds the critical value, the dislocation slip will be activated in adjacent grains, then macro yielding will occur when $\gamma = \rho v b$, where v is dislocation velocity and b is the Burgers vector, is satisfied. In coarse grains, large number of dislocations can be accumulated, leading to greater stress concentration, so the flow stress value required for macro yielding is lower [24,57]. For the model material, Ti–30Zr–5Mo, its Hall-Petch coefficient (k) reaches 720 MPa μm$^{-1/2}$ (Fig. 13 (a)). As shown in Fig. 13 (b), Hall-Petch coefficient (k) in the β Ti alloys were generally divided into k for dislocation slip, k for twinning, and k for phase transformation, with lower k values for slip and higher k values for phase transformation [17,39–42]. The k for phase transformation in the Ti–30Zr–5Mo materials is much larger than that for dislocation slip. According to Fig. 11, the martensite α' are regarded to activate before the macroscopic yielding which is similar to the twinning in the Ti–15Mo alloy [17], and the occurrence of martensitic transformation can reduce the stress concentration as other research reported [43]. On the other hand, α' phase is more easily formed in coarse grains shown in

Fig. 11(a and b), and under the same strain, the Kernel average misorientation (KAM) value at the α'/β phase interface is higher than that at grain boundaries shown in Fig. 11(c and d). The α'/β phase interface disperses the local stress concentration that should occur at the β/β grain boundaries. The above factors contribute to the fluctuation of the trigger stress. Even with fluctuation, grain refinement is effective to improve the trigger stress of the materials.

The systematic Gibbs free energy changes during SIMT in metastable β titanium alloys may explain trigger stress fluctuation from thermodynamic perspective. The effect of grain size on trigger stress can be explained by the equation [44]:

$$\Delta G = (\Delta H - T\Delta S) + \Delta E_{el} + \delta E_{irr} - \frac{1}{\rho}\sigma\varepsilon_{tr} - \frac{1}{2\rho}\left[\left(\frac{\sigma^2}{E_M}\right) - \left(\frac{\sigma^2}{E_\beta}\right)\right] \quad (7)$$

where ΔH is the change in enthalpy, T is the test temperature, ΔS is the entropy change, $(\Delta H - T\Delta S)$ is the change in chemical free energy in the process of SIMT, ΔE_{el} is the internal elastic energy stored in the β phase due to formation of α' phase, δE_{irr} is the irreversible work consumed in overcoming internal frictional resistances to phase boundary movement, ρ is the density of the β phase, ε_{tr} is the transformation strain determined by lattice distortion of α' phase in the direction of stress, E_M and E_β are the Young's moduli of the martensite and β phases, respectively, and $\frac{1}{2\rho}\left[\left(\frac{\sigma^2}{E_M}\right) - \left(\frac{\sigma^2}{E_\beta}\right)\right]$ is the elastic energy created due to external stress and the elastic elongation owing to the difference in elastic moduli of β and α' phase. Eq. (7) shows that the changes in enthalpy and entropy are independent of the grain size, so the free energy change during the martensite phase transformation is not affected by the grain size. However, as the grain size changes, the friction energy and elastic energy terms show opposite trends [45]. This is because the average length and width of the stress-induced martensite depend on the average grain size of the β phase. The average lath size of the martensite in larger grains would always be higher than in the small grains. The martensite size change in the different grain size in the present alloy is clearly evident in Fig. 13 (b). Since the frictional resistance is proportional to the volume swept by the interface, i.e., the volume of the SIM, the larger will be the plate length and width, the smaller will be the total β/α'
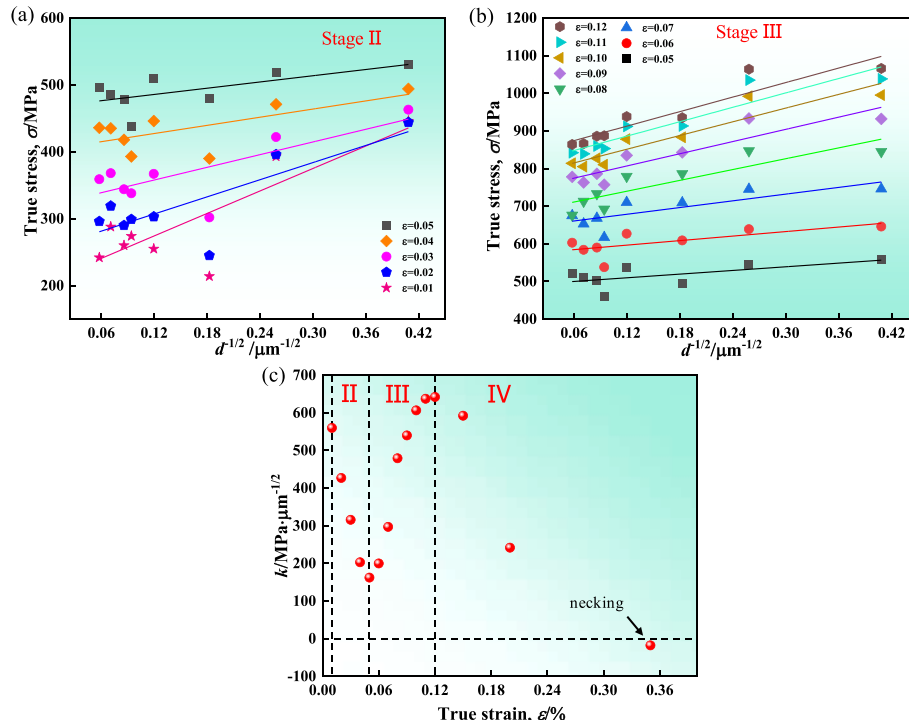

Fig. 13. Hall-Petch coefficient (k) of (a) Ti–30Zr–5Mo alloy and (b) other different titanium alloys [17,39–42].

interfacial area. For a given volume fraction of martensite, an increase in grain size results in a decrease in δE_{irr} in overcoming the internal friction resistance. In addition, the internal stress field in the β phase is affected by the size of martensite phase. For a given volume of martensite, the decrease in plate size reduces the intensity and size of region, over which the stress field is generated, hence, ΔE_{el}. As mentioned above, the mean length and width of martensitic plates are expected to increase with an increase in grain size. Thus, the larger the grain size will be, the higher will be the stress field and, hence, the higher the stored internal elastic energy (ΔE_{el}). Therefore, ΔE_{el} increases with an increase in grain size, whereas δE_{irr} decreases. For the small grain sizes, δE_{irr} plays a dominant role in the change in the trigger stress, while in large grains, ΔE_{el} becomes dominant [46]. Further, grain size is also not expected to affect the modulus or density and, hence, the last two terms in Eq. (7). This is one of the reasons for the fluctuation of the trigger stress for SIMT with decreasing grain size in the Ti–30Zr–5Mo alloy.

4.4. Relationship between deformation-induced phase transformation and strain hardening rate

To further understand the deformation behavior, the Hall-Petch relationship between the flow stress and the inverse square root of the static grain size in the stage II and III is statistically calculated based on empirical form, as shown in Fig. 14(a and b) [17]. Combining the Hall-Petch equation ($\sigma = \sigma_0 + kd^{-\frac{1}{2}}$, where σ_0 is the constant) [12] with the stress-strain curves of the Ti–30Zr–5Mo alloy (Fig. 5) and its Hall-Petch coefficient (k) variation curves in stage II and III (Fig. 14a–(b)), it can be seen that in the stage II, the Hall-Petch coefficient continuously decreases with the increase of strain, while the stress increases. Therefore, the inverse square root of the static grain size ($d^{1/2}$) continuously increases with the increase of strain, which means that the n size (d) decreases, indicating the occurrence of dynamic refinement. In the stage III, as strain increases, the Hall-Petch coefficient continues to increase, while the stress also increases with the strain. Therefore, at this stage, the dynamic refinement effect becomes weaker. As shown in Fig. 14 (a) in the stage II, the Hall-Petch coefficient of the Ti–30Zr–5Mo alloy at each strain gradually decreases from 560 to 162 MPa μm$^{-1/2}$, which also proves that α′ martensite rapidly grows and penetrates β grain size in the stage II during this process. In the stage III, the

Hall-Petch coefficient (k) of Ti–30Zr–5Mo alloy at each strain begins to increase from 162 to 642 MPa μm$^{-1/2}$, indicating that α′ martensite has almost reached saturation during this process.

In addition to grain boundaries, phase boundaries also play a similar role in the Hall-Petch coefficient (k) of the Ti–30Zr–5Mo alloy with phase transformation [39]. The obvious formation of α′ martensite can also be found in the in-situ SEM images of Fig. 12(a and b). This also indicates that the variation of the Hall-Petch coefficient (k) is probably influenced by the α′ martensite phase interfaces as the flow stress increases. In addition, the α′ martensite in Fig. 12(c and d) again confirms that the α′ saturation process occurs in II to III stages of the work hardening rate curve. As shown in Fig. 15 (a), before the formation of α′ martensite, only the β/β grain boundaries hindered the movement of dislocations. At this time, stress concentration occurred at the β/β grain boundaries, which induced the formation of α′ martensite and formed a longer dislocation free path. As the strain increases, α′ martensite penetrates β grains, the formed α′/β phase boundaries hindering the movement of dislocations shorten the free path of dislocations. When α′ martensite is saturated, α′ martensite becomes the predominant phase of the grain, and the α′/α' phase boundaries become the main barrier that hinders the movement of dislocations, resulting in an increase in the free path of dislocations. To obtain the morphology and distribution of α′ and β phase, EBSD analysis of 15 μm material is represented in Fig. 15(b–e). With the increase of flow stress, besides β/β grains boundaries, dislocation movement also can be hindered at the α′/β phase boundaries and geometrically necessary dislocations can be found. As the α′ phase widens gradually, the mean free path of dislocations in the β grains decreases, resulting in a strong work hardening ability at stage II. As the α′ phase gradually saturates and the grains are occupied by the α′ phase, the increase of dislocation mean free path in the α′ grain causes the decrease of work hardening effect in stage III.

The formation of SIMT during the deformation of fine and coarse grains can explain the change of work hardening behavior. The fine grains disperse more local dislocation stress concentration than the coarse grains and have more grain boundaries and β/α′ interfacial area [47–49]. Therefore, assuming grain size is homogenous, there will be more β/α′ interfacial area and martensite nucleation in the fine grains than coarse grains with the increase of applied stress, the boundaries hardening and stress filed hardening caused by martensite both
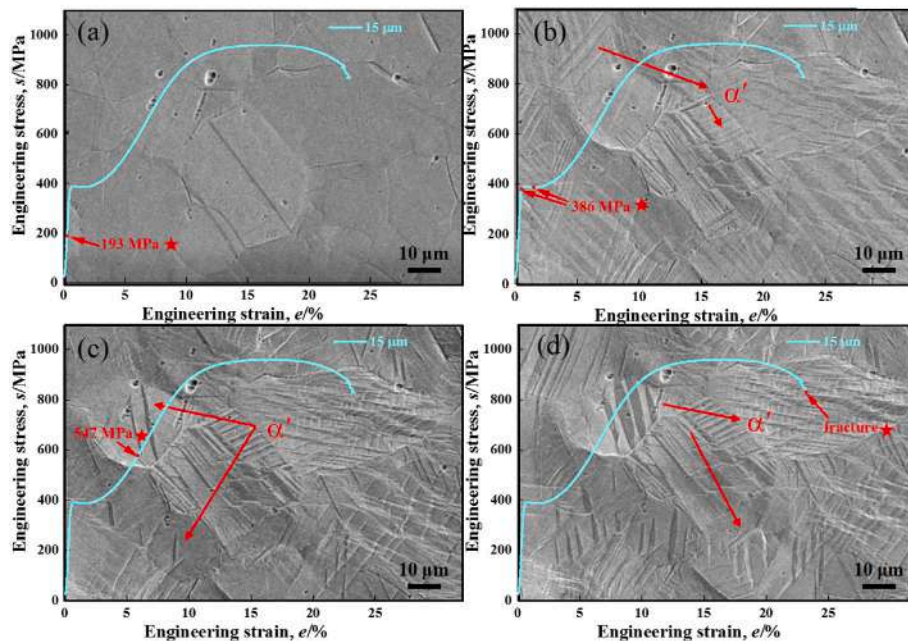

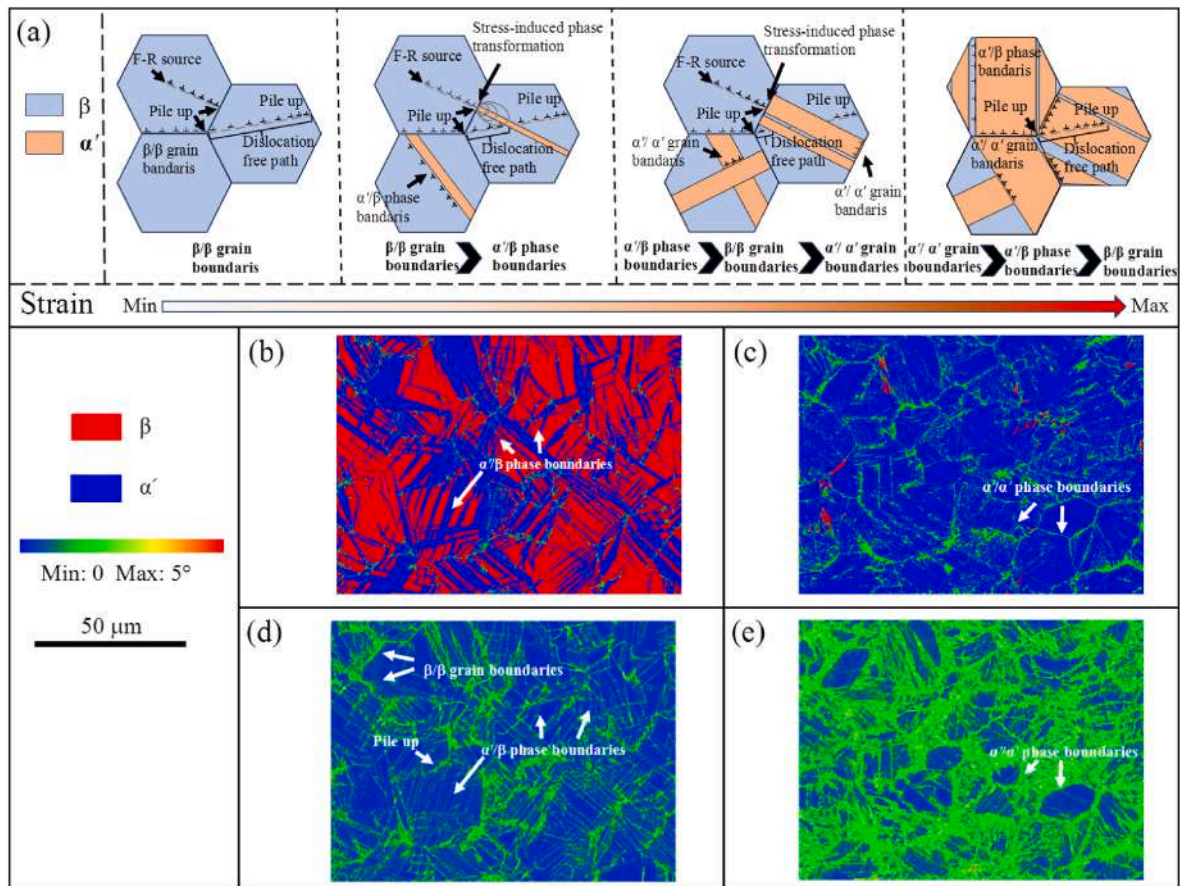**Fig. 14.** Hall-Petch relationship between flow stress and inverse square root of the static grain size in the Ti–30Zr–5Mo alloy at (a) stage II and (b) stage III, and (c) evolution of Hall-Petch coefficient at each strain in the Ti–30Zr–5Mo alloy.

Fig. 15. (a) Mechanism diagram showing β/β grain boundaries, α′/β phase boundaries, and α′/α′ grain boundaries hindering dislocation movement with increasing stress in the Ti–30Zr–5Mo alloy. (b) and (c) In-situ EBSD phase maps at 3% and 10% strains. (d) and (e) KAM maps corresponding to (b) and (c).

contribute the stronger work hardening ability in the fine-grained material.

5. Conclusions

In this study, a series of Ti–30Zr–5Mo materials with different β grain sizes were prepared through applying cold-working and annealing. The effect of β grain size on the deformation behavior and mechanical properties of the alloy was investigated. The main conclusions can be summarized as follows:

(1) A large β grain size change ranging from 6 to 475 μm has be prepared by SIMRT and simple heat treatments. The grain size is more sensitive to annealing temperature than time duration, and SIMRT is an effective way to refine the metastable β alloy.

(2) All stress-strain curves of the Ti–30Zr–5Mo materials with the different grain sizes ranging from 6 to 475 μm exhibit double yielding phenomena. Stress induced α′ martensitic transformation occurs in all the materials. The grain size has little effect on the transformed α′ phase amount.

(3) The Hall-Petch coefficient for martensite transformation of the Ti–30Zr–5Mo alloy reaches 720 MPa μm$^{-1/2}$, indicating that the trigger stress is strongly dependent on the grain size.

(4) With the increase of flow stress, the α′/β phase boundaries and α′/α' grain boundaries become effective barriers for dislocation movement. The variation of the mean free path of dislocations can cause the variation of work hardening ability and Hall-Petch coefficient value of the Ti–30Zr–5Mo materials.

(5) The trigger stress can be adjusted between 211 and 464 MPa by controlling the grain size. Even with a high trigger stress of 464 MPa in the material with an average grain size of 6 μm, an excellent ductility of 21% is obtained. The material with a grain size of 113 μm shows the excellent comprehensive mechanical properties with an SDI value of 252 MPa.

CRediT authorship contribution statement

Chenyang Wu: Writing – original draft, Investigation. **Xiaoli Zhao:** Writing – review & editing, Writing – original draft, Project administration, Funding acquisition, Conceptualization. **Mengrui Zhang:** Methodology, Investigation. **Hideki Hosoda:** Writing – review & editing, Supervision. **Takayoshi Nakano:** Writing – review & editing, Funding acquisition. **Mitsuo Niinomi:** Supervision, Writing – review & editing. **Nan Jia:** Funding acquisition, Writing – review & editing. **Zhiwen Shao:** Methodology, Supervision, Writing – review & editing. **Deliang Zhang:** Supervision, Validation, Writing – review & editing.

Declaration of competing interest

The authors declare that they have no known competing financial interests or personal relationships that could have appeared to influence the work reported in this paper.

Data availability

Data will be made available on request.

References

[1] J. Gao, Y. Huang, D. Guan, A.J. Knowles, L. Ma, D. Dye, W.M. Rainforth, Deformation mechanisms in a metastable beta titanium twinning induced plasticity alloy with high yield strength and high strain hardening rate, Acta Mater. 152 (2018) 301–314, https://doi.org/10.1016/J.ACTAMAT.2018.04.035.

[2] S. Ozan, J. Lin, Y. Zhang, Y. Li, C. Wen, Cold rolling deformation and annealing behavior of a β-type Ti–34Nb–25Zr titanium alloy for biomedical applications, J. Mater. Res. Technol. 9 (2020) 2308–2318, https://doi.org/10.1016/J.JMRT.2019.12.062.

[3] L. Shao, W. Li, D. Li, G. Xie, C. Zhang, C. Zhang, J. Huang, A review on combustion behavior and mechanism of Ti alloys for advanced aero-engine, J. Alloys Compd. 960 (2023) 170584, https://doi.org/10.1016/J.JALLCOM.2023.170584.

[4] D. Banerjee, J.C. Williams, Perspectives on titanium science and technology, Acta Mater. 61 (2013) 844–879, https://doi.org/10.1016/J.ACTAMAT.2012.10.043.

[5] X. Ji, I. Gutierrez-Urrutia, S. Emura, T. Liu, T. Hara, X. Min, D. Ping, K. Tsuchiya, Twinning behavior of orthorhombic-α" martensite in a Ti-7.5Mo alloy, Sci. Technol. Adv. Mater. 20 (2019) 401–411, https://doi.org/10.1080/14686996.2019.1600201.

[6] B. Qian, J. Zhang, Y. Fu, F. Sun, Y. Wu, J. Cheng, P. Vermaut, F. Prima, In-situ microstructural investigations of the TRIP-to-TWIP evolution in Ti-Mo-Zr alloys as a function of Zr concentration, J. Mater. Sci. Technol. 65 (2021) 228–237, https://doi.org/10.1016/J.JMST.2020.04.078.

[7] X. Zhao, M. Niinomi, M. Nakai, T. Ishimoto, T. Nakano, Development of high Zr-containing Ti-based alloys with low Young's modulus for use in removable implants, Mater. Sci. Eng. C 31 (2011) 1436–1444, https://doi.org/10.1016/j.msec.2011.05.013.

[8] Y. Chong, R. Gholizadeh, T. Tsuru, R. Zhang, K. Inoue, W. Gao, A. Godfrey, M. Mitsuhara, J.W. Morris, A.M. Minor, N. Tsuji, Grain refinement in titanium prevents low temperature oxygen embrittlement, Nat. Commun. 14 (2023) 404, https://doi.org/10.1038/s41467-023-36030-0.

[9] N. Tsuji, Y. Ito, Y. Saito, Y. Minamino, Strength and ductility of ultrafine grained aluminum and iron produced by ARB and annealing, Scr. Mater. 47 (2002) 893–899, https://doi.org/10.1016/S1359-6462(02)00282-8.

[10] Q. Yuan, J. Ren, J. Mo, Z. Zhang, E. Tang, G. Xu, Z. Xue, Effects of rapid heating on the phase transformation and grain refinement of a low-carbon microalloyed steel, J. Mater. Res. Technol. 23 (2023) 3756–3771, https://doi.org/10.1016/j.jmrt.2023.02.018.

[11] T.G. Langdon, The principles of grain refinement in equal-channel angular pressing, Mater. Sci. Eng. A 462 (2007) 3–11, https://doi.org/10.1016/j.msea.2006.02.473.

[12] X.J. Jiang, H.T. Zhao, R.H. Han, X.Y. Zhang, M.Z. Ma, R.P. Liu, Grain refinement and tensile properties of a metastable TiZrAl alloy fabricated by stress-induced martensite and its reverse transformation, Mater. Sci. Eng. A 722 (2018) 8–13, https://doi.org/10.1016/J.MSEA.2018.02.104.

[13] A. Di Schino, M. Barteri, J.M. Kenny, Development of ultra fine grain structure by martensitic reversion in stainless steel, J. Mater. Sci. Lett. 21 (2002) 751–753, https://doi.org/10.1023/A:1015757710546.

[14] Y. Ma, J.E. Jin, Y.K. Lee, A repetitive thermomechanical process to produce nano-crystalline in a metastable austenitic steel, Scr. Mater. 52 (2005) 1311–1315, https://doi.org/10.1016/J.SCRIPTAMAT.2005.02.018.

[15] A. Bhattacharjee, S. Bhargava, V.K. Varma, S. V Kamat, A.K. Gogia, Effect of β grain size on stress induced martensitic transformation in β solution treated Ti-10V-2Fe-3Al alloy, Scr. Mater. 53 (2005) 195–200, https://doi.org/10.1016/j.scriptamat.2005.03.039.

[16] M.H. Cai, C.Y. Lee, Y.K. Lee, Effect of grain size on tensile properties of fine-grained metastable β titanium alloys fabricated by stress-induced martensite and its reverse transformations, Scr. Mater. 66 (2012) 606–609, https://doi.org/10.1016/J.SCRIPTAMAT.2012.01.015.

[17] K. Yao, X. Min, Static and dynamic Hall−Petch relations in {332}<113> TWIP Ti–15Mo alloy, Mater. Sci. Eng. A 827 (2021) 142044, https://doi.org/10.1016/J.MSEA.2021.142044.

[18] X. Zhao, Y. Wang, H. Xue, N. Jia, Y. Liu, D. Zhang, The effect of strain rate on deformation-induced α′ phase transformation and mechanical properties of a metastable β-type Ti–30Zr–5Mo alloy, J. Alloys Compd. 894 (2022) 162394, https://doi.org/10.1016/J.JALLCOM.2021.162394.

[19] A. Paradkar, S.V. Kamat, The effect of strain rate on trigger stress for stress-induced martensitic transformation and yield strength in Ti–18Al–8Nb alloy, J. Alloys Compd. 496 (2010) 178–182, https://doi.org/10.1016/J.JALLCOM.2010.02.106.

[20] K. Yuan, Y. Jiang, S. Liu, S. Xu, X. Li, X. Wu, Effect of carbon upon mechanical properties and deformation mechanisms of TWIP and TRIP-assisted high entropy alloys, Mater. Sci. Eng. A 857 (2022) 144126, https://doi.org/10.1016/J.MSEA.2022.144126.

[21] S.S. Nene, K. Liu, M. Frank, R.S. Mishra, R.E. Brennan, K.C. Cho, Z. Li, D. Raabe, Enhanced strength and ductility in a friction stir processing engineered dual phase high entropy alloy, Sci. Rep. 7 (2017) 16167, https://doi.org/10.1038/s41598-017-16509-9.

[22] L. Ren, W. Xiao, C. Ma, R. Zheng, L. Zhou, Development of a high strength and high ductility near β-Ti alloy with twinning induced plasticity effect, Scr. Mater. 156 (2018) 47–50, https://doi.org/10.1016/J.SCRIPTAMAT.2018.07.012.

[23] X. Min, P. Bai, S. Emura, X. ji, C. Cheng, B. Jiang, K. Tsuchiya, Effect of oxygen content on deformation mode and corrosion behavior in β-type Ti-Mo alloy, Mater. Sci. Eng. A 684 (2017) 534–541, https://doi.org/10.1016/J.MSEA.2016.12.062.

[24] S. Sadeghpour, S.M. Abbasi, M. Morakabati, A. Kisko, L.P. Karjalainen, D.A. Porter, A new multi-element beta titanium alloy with a high yield strength exhibiting transformation and twinning induced plasticity effects, Scr. Mater. 145 (2018) 104–108, https://doi.org/10.1016/J.SCRIPTAMAT.2017.10.017.

[25] X. Ma, Z. Chen, L. Xiao, W. Lu, S. Luo, Y. Mi, Compressive deformation of a metastable β titanium alloy undergoing a stress-induced martensitic transformation: the role of β grain size, Mater. Sci. Eng. A 794 (2020) 139919, https://doi.org/10.1016/J.MSEA.2020.139919.

[26] D. Das, P.P. Chattopadhyay, Influence of martensite morphology on the work-hardening behavior of high strength ferrite-martensite dual-phase steel, J. Mater. Sci. 44 (2009) 2957–2965, https://doi.org/10.1007/s10853-009-3392-0.

[27] G. Dini, A. Najafizadeh, R. Ueji, S.M. Monir-Vaghefi, Tensile deformation behavior of high manganese austenitic steel: the role of grain size, Mater. Des. 31 (2010) 3395–3402, https://doi.org/10.1016/J.MATDES.2010.01.049.

[28] Z. Jiang, Z. Guan, J. Lian, Effects of microstructural variables on the deformation behaviour of dual-phase steel, Mater. Sci. Eng. A 190 (1995) 55–64, https://doi.org/10.1016/0921-5093(94)09594-M.

[29] C. Li, L. Huang, C. Li, S. Hui, Y. Yu, M. Zhao, S. Guo, J. Li, Research progress on hot deformation behavior of high-strength β titanium alloy: flow behavior and constitutive model, Rare Met. 41 (2022) 1434–1455, https://doi.org/10.1007/s12598-021-01861-7.

[30] C. Zhu, X. Zhang, C. Li, C. Liu, K. Zhou, A strengthening strategy for metastable β titanium alloys: synergy effect of primary α phase and β phase stability, Mater. Sci. Eng. A 852 (2022) 143736, https://doi.org/10.1016/J.MSEA.2022.143736.

[31] F.J. Gil, J.A. Planell, Behaviour of normal grain growth kinetics in single phase titanium and titanium alloys, Mater. Sci. Eng. A 283 (2000) 17–24, https://doi.org/10.1016/S0921-5093(00)00731-0.

[32] H. Zhiguo, Chen Yuyong, The effect of trace TiB2 on the grain growth kinetics of Ti–6Al–4V alloy in the β phase region, J. Funct. Mater. 2 (2016) 2094–2099, https://doi.org/10.3969/j.issn.1001-9731.2016.02.019.

[33] T. Wang, H. Guo, L. Tan, Z. Yao, Y. Zhao, P. Liu, Beta grain growth behaviour of TG6 and Ti17 titanium alloys, Mater. Sci. Eng. A 528 (2011) 6375–6380, https://doi.org/10.1016/J.MSEA.2011.05.042.

[34] P.G. Shewmon, T.P.G. Shewmon, Transformation in Metal, McGraw-Hill, 1969. https://api.semanticscholar.org/CorpusID:135940875.

[35] X. Ma, F. Li, J. Cao, J. Li, Z. Sun, G. Zhu, S. Zhou, Strain rate effects on tensile deformation behaviors of Ti–10V–2Fe–3Al alloy undergoing stress-induced martensitic transformation, Mater. Sci. Eng. A 710 (2018) 1–9, https://doi.org/10.1016/J.MSEA.2017.10.057.

[36] Y.Z. Tian, S. Gao, L.J. Zhao, S. Lu, R. Pippan, Z.F. Zhang, N. Tsuji, Remarkable transitions of yield behavior and Lüders deformation in pure Cu by changing grain sizes, Scr. Mater. 142 (2018) 88–91, https://doi.org/10.1016/J.SCRIPTAMAT.2017.08.034.

[37] W. Mao, S. Gao, W. Gong, Y. Bai, S. Harjo, M.H. Park, A. Shibata, N. Tsuji, Quantitatively evaluating respective contribution of austenite and deformation-induced martensite to flow stress, plastic strain, and strain hardening rate in tensile deformed TRIP steel, Acta Mater. 256 (2023) 119139, https://doi.org/10.1016/J.ACTAMAT.2023.119139.

[38] R. Sarkar, A. Mukhopadhyay, P. Ghosal, T.K. Nandy, K.K. Ray, A study on anomalous yield drop behaviour in modified beta titanium alloys, Philos. Mag. A 100 (2020) 399–425, https://doi.org/10.1080/14786435.2019.1687950.

[39] A.G. Paradkar, S.V. Kamat, A.K. Gogia, B.P. Kashyap, On the validity of Hall–Petch equation for single-phase β Ti–Al–Nb alloys undergoing stress-induced martensitic transformation, Mater. Sci. Eng. A 520 (2009) 168–173, https://doi.org/10.1016/J.MSEA.2009.05.041.

[40] X. Huang, J.S. Li, M.J. Lai, Influences of grain size on the deformation behavior of a twinning-induced plasticity metastable β titanium alloy, J. Alloys Compd. 937 (2023) 168274, https://doi.org/10.1016/J.JALLCOM.2022.168274.

[41] B. Jiang, S. Emura, K. Tsuchiya, Microstructural evolution and its effect on the mechanical behavior of Ti–5Al–5Mo–5V–3Cr alloy during aging, Mater. Sci. Eng. A 731 (2018) 239–248, https://doi.org/10.1016/J.MSEA.2018.06.064.

[42] W.L. Wang, X.L. Wang, W. Mei, J. Sun, Role of grain size in tensile behavior in twinning-induced plasticity β Ti–20V–2Nb–2Zr alloy, Mater. Charact. 120 (2016) 263–267, https://doi.org/10.1016/J.MATCHAR.2016.09.016.

[43] Y. Danard, G. Martin, L. Lilensten, F. Sun, A. Seret, R. Poulain, S. Mantri, R. Guillou, D. Thiaudière, I. Freiherr von Thüngen, D. Galy, M. Piellard, N. Bozzolo, R. Banerjee, F. Prima, Accommodation mechanisms in strain-transformable titanium alloys, Mater. Sci. Eng. A 819 (2021) 141437, https://doi.org/10.1016/J.MSEA.2021.141437.

[44] Y. Liu, H. Yang, The concern of elasticity in stress-induced martensitic transformation in NiTi, Mater. Sci. Eng. A 260 (1999) 240–245, https://doi.org/10.1016/S0921-5093(98)00959-9.

[45] A. Bhattacharjee, V.K. Varma, S. V Kamat, A.K. Gogia, S. Bhargava, Influence of β grain size on tensile behavior and ductile fracture toughness of titanium alloy Ti–10V–2Fe–3Al, Metall. Mater. Trans. A 37 (2006) 1423–1433, https://doi.org/10.1007/s11661-006-0087-x.

[46] H. Sakamoto, Distinction between thermal and stress-induced martensitic transformations and inhomogeneity in internal stress, Mater. Trans. 43 (2002) 2249–2255, https://doi.org/10.2320/matertrans.43.2249.

[47] S. Sadeghpour, S.M. Abbasi, M. Morakabati, Deformation-induced martensitic transformation in a new metastable β titanium alloy, J. Alloys Compd. 650 (2015) 22–29, https://doi.org/10.1016/J.JALLCOM.2015.07.263.

[48] S. Kajiwara, Roles of dislocations and grain boundaries in martensite nucleation, Metall. Trans. A. 17 (1986) 1693–1702, https://doi.org/10.1007/BF02817268.

[49] X. Ma, H. Zhai, L. Song, W. Zhang, Y. Hu, Q. Zhang, In situ study on plastic deformation mechanism of Al0.3CoCrFeNi high-entropy alloys with different microstructures, Mater. Sci. Eng. A. 857 (2022) 144134, https://doi.org/10.1016/J.MSEA.2022.144134.